What controls equatorial Atlantic winds in boreal spring?

INGO RICHTER, SWADHIN K. BEHERA, AND TAKESHI DOI

Research Institute for Global Change and Application Laboratory, JAMSTEC, Yokohama, Japan, and Application Laboratory, JAMSTEC, Yokohama Japan

BUNMEI TAGUCHI

Earth Simulator Center, JAMSTEC, Yokohama, Japan

YUKIO MASUMOTO

Research Institute for Global Change, JAMSTEC, Yokohama, Japan

SHANG-PING XIE

Scripps Institution of Oceanography, University of California at San Diego, La Jolla, California, USA

Climate Dynamics

submitted, 26 September 2013

revised, 24 April 2014

Corresponding author address:

Ingo Richter

Research Institute for Global Change, JAMSTEC, 3173-25 Showa-machi, Kanazawa-ku, Yokohama, Kanagawa 236-0001, Japan

E-mail: richter@jamstec.go.jp

ABSTRACT

The factors controlling equatorial Atlantic winds in boreal spring are examined using both observations and general circulation model (GCM) simulations from the Coupled Model Intercomparison Phase 5 (CMIP5). The results show that the prevailing surface easterlies flow against the attendant pressure gradient and must therefore be maintained by other terms in the momentum budget. An important contribution comes from meridional advection of zonal momentum but the dominant contribution is the vertical transport of zonal momentum from the free troposphere to the surface. This implies that surface winds are strongly influenced by conditions in the free troposphere, chiefly pressure gradients and, to a lesser extent, meridional advection. Both factors are linked to the patterns of deep convection. This implies that, consistent with the results of previous studies, the persistent westerly surface wind bias found in most GCMs is due mostly to precipitation errors, in particular excessive precipitation south of the equator over the ocean and deficient precipitation over equatorial South America.

Free tropospheric influences also dominate the interannual variability of surface winds in boreal spring. GCM experiments with prescribed climatological sea-surface temperatures (SSTs) indicate that the free tropospheric influences are mostly associated with internal atmospheric variability. Since the surface wind anomalies in boreal spring are crucial to the development of warm SST events (Atlantic Niños), the results imply that interannual variability in the region may rely far less on coupled air-sea feedbacks than is the case in the tropical Pacific.

1. Introduction

Surface winds are crucial for air-sea interaction because they control turbulent fluxes of heat and momentum at the air-sea interface. Areas of particular interest are the equatorial Pacific and Atlantic Oceans where surface easterly winds drive westward currents and upwelling that play a crucial role in the distribution of ocean temperatures both at the surface and below. Salient features include the western warm pool, eastern cold tongue, and a thermocline that slopes upward toward the east.

Variations in surface winds underlie a wide range of coupled ocean-atmosphere phenomena that operate on intraseasonal to decadal timescales. Probably most prominent among these is the El Niño-Southern Oscillation (ENSO; Philander 1990; Neelin et al. 1998) in the equatorial Pacific due to its dominant influence across the globe (Wallace et al. 1992; Alexander et al. 2002). A similar phenomenon in the Atlantic has been named Atlantic Niño due to its apparent similarity with ENSO (Zebiak 1993) though recent results suggest that off-equatorial influences are also important there (Foltz and McPhaden 2010; Lübbecke and McPhaden 2012; Richter et al. 2013).

While the surface winds exert a crucial influence on the ocean, the ocean also influences the surface winds in profound ways (Bjerknes 1969; Wallace et al. 1989; Chelton et al. 2001; Xie 2004) through the sea-surface temperatures (SSTs), which modify surface stability, atmospheric convection, and surface pressure. The zonal SST gradient in the equatorial Pacific, for example, sets up a surface pressure gradient that drives easterly winds and thus reinforces the SST gradient, a coupled process known as the Bjerknes feedback.

While the influence of SST on surface winds is indisputable, the exact extent to which tropical surface winds are determined by the underlying SST patterns remains under discussion. An influential paper by Gill (1980) presented an analytical two-layer shallow water model of the atmospheric response to prescribed diabatic heating (Gill model hereafter). This has inspired a paradigm, in which surface winds are considered a response to free tropospheric heating. In contrast, Lindzen and Nigam (1987; LN87 hereafter) devised a one-layer model of the atmospheric boundary layer (LN model hereafter), in which the surface pressure field was entirely determined by the underlying SST. This model was reasonably successful in reproducing some observed features and has thus inspired another paradigm in which surface winds are largely determined by the underlying SST distribution. Which influence on surface winds is dominant has important implications for our concept of tropical air-sea interaction. The Gill model emphasizes the influence of an elevated heat source and thus allows for remote effects, e.g. from the continents (Gill's paper was inspired by the idea that convection over the maritime continent drives the surface easterlies over the equatorial Pacific) or from the subtropics. The LN model, on the other hand, presents a view, in which atmospheric winds are dominated by the underlying SST, and thus suggests a tighter coupling between atmosphere and ocean. Several studies have assessed the validity of the two views and there seems to be a consensus that meridional winds are dominated by SST gradients, while zonal winds are dominated by free tropospheric heating (Chiang et al. 2001; Back and Bretherton 2009a,b).

What controls equatorial surface winds might also have important implications for understanding general circulation model (GCM) biases. Particularly in the equatorial Atlantic GCMs suffer from a persistent westerly surface wind bias in boreal spring (Richter and Xie 2008; Richter et al. 2014), which severely affects the simulated mean state (Davey et al. 2002; Richter and Xie 2008), interannual variability (Richter et al. 2014), and seasonal predictions (Stockdale et al. 2006). Several studies have shown that these westerly wind biases are nascent in atmospheric GCM

(AGCM) simulations with SSTs prescribed from observations and that precipitation errors over the adjacent continents might play a role (Chang et al. 2007 and 2008; Richter et al. 2008, Richter et al. 2012; Zermeno and Zhang 2013). The latter view is consistent with the Gill paradigm, in which continental convection can play an important role in marine surface winds. If the LN paradigm is correct, on the other hand, the Atlantic biases should be seen as a coupled phenomenon in which initial small errors get amplified by air-sea feedbacks.

In the present study we examine the factors controlling surface winds over the equatorial Atlantic Ocean. More specifically, we would like to address the following questions: 1) What controls the climatological mean winds? 2) What controls interannual variability of the surface winds and what are the consequences for coupled phenomena like the Atlantic Niño? 3) Can the answers to the two previous questions help us understand the persistent westerly bias in GCMs?

Our analysis focuses on the March-April-May (MAM) season for several reasons. First, it is the season when the zonal equatorial SST gradient is weakest (Okumura and Xie 2004) and should have the smallest impact on surface winds according to the LN model. This should bring to the fore other influences on the surface winds, if such influences do exist. Second, the observed intertropical convergence zone (ITCZ) is closest to the equator in MAM. This allows studying the influence of deep convection on surface winds at the equator, an aspect not addressed by many studies of tropical surface winds (Lindzen and Nigam 1987; Chiang et al. 2001; Stevens et al. 2002; Back and Bretherton 2009a, BB09 hereafter). Third, the GCM surface wind biases are most pronounced in MAM.

The rest of the paper is organized as follows. In section 2 we introduce the observational data and model output used in this study. We also describe the atmospheric mixed layer model (MLM) introduced by Stevens et al. (2002) and modified by BB09, which will be one of our diagnostic tools. Section 3 examines the factors controlling the mean state winds in observations and models. In section 4 we analyze the factors controlling interannual variability of the surface winds and relates these to the results of section 3. Using the results from sections 3 and 4 we examine the GCM westerly bias problem in section 5. In section 6 we summarize our results and present our conclusions.

2. Observational data, model description and methods

2.1. Data

Surface wind data in this study is from satellite (QuikSCAT; period 2000-2009; Dunbar et al. 2006) and shipboard observations (ICOADS; period 1960-2012; Woodruff et al. 2011). The latter also provides the sea-level pressure observations used in this study. Precipitation for the period 1979-2012 is from the Global Precipitation Climatology Project (GPCP) version 2.2, which is a blend of station and satellite data (Adler et al. 2003).

In the present study we are interested in a three-dimensional view of equatorial winds, and the boundary layer and free tropospheric processes that maintain them. To obtain a view of the three dimensional circulation patterns that give rise to the surface winds we rely on reanalysis data, while keeping in mind that these really represent a blend of observational data and GCM output. The reanalysis dataset used is the European Center for Medium Range Weather Forecasts (ECMWF) Interim Analysis (ERA-Int hereafter; Dee et al. 2011) for the period 1989 to 2012.

2.2. GCMs

The GCM output analyzed in this study is from the Coupled Model Intercomparison Project phase 5 (CMIP5) that was performed in preparation for the 5th assessment report (AR5) of the Intergovernmental Panel on Climate Change (IPCC). Our focus is on the factors controlling fundamental model behavior and thus we chose the pre-industrial control simulation (piControl hereafter) because of its stable greenhouse gas forcing and long integration periods. In order to isolate coupled air-sea versus intrinsic atmospheric processes we also examine uncoupled AGCM-only runs with SST prescribed from each model's climatology (experiment climSST). Despite the stable external forcing climate drift may exist in some models. We therefore remove the long-term linear trend from all fields for our analysis of interannual variability. This is also performed for the observational and reanalysis datasets, where fields show a noticeable trend over the last few decades.

For our analysis we choose the 12 GCMs that performed both experiments used in our analysis (piControl and climSST; Table 1), which allows comparison of consistent ensemble averages. While the CMIP5 archive currently contains more than 40 GCMs for piControl, this 12-model sample is reasonably representative in the sense that the equatorial Atlantic SST biases in these GCMs approximately span the range of the piControl models. The ensemble also features a wide range of behaviors regarding their simulated zonal modes (see Richter et al. 2014 for an evaluation of a large sample of piControl models).

2.3. Diagnostic methods

Stevens et al. (2002) have devised a diagnostic model of the surface (or boundary layer) winds that uses as its starting point the three-way (Ekman) balance among pressure gradient force, Coriolis force, and surface drag (e.g. Deser 1993) for a planetary boundary layer (PBL) of constant depth. To this they add a simple formulation of vertical entrainment at the PBL top to arrive at the generalized Ekman balance

$$f\mathbf{k}\times\mathbf{U} + \alpha_0 \nabla p = -\mathbf{U} \parallel \mathbf{U} \parallel \frac{C_D}{h} + (\mathbf{U}_T - \mathbf{U})\frac{w_e}{h} \quad (1)$$

where $\alpha_0 \equiv 1/\rho_0$ is the basic state specific volume, **U** the PBL wind vector, C_D the drag coefficient, $\mathbf{U}_T$ the free tropospheric wind entrained into the PBL, and w_e the entrainment velocity. Stevens et al. (2002) and BB09 interpret h as the depth over which momentum is well mixed, which is typically the subcloud layer in the deep tropics. Equation (1) neglects meridional advection, which is thought to be important for the equatorial momentum balance (Okumura and Xie 2004). For our analysis of the equatorial surface wind budget we therefore add advection and, by neglecting the coriolis term, arrive at the following equation for zonal surface momentum

$$\frac{\partial U}{\partial t} + U\frac{\partial U}{\partial x} + V\frac{\partial U}{\partial y} + \alpha_0 \frac{\partial p}{\partial x} = -\frac{\tau_x}{h} + (U_T - U)\frac{w_e}{h} \quad (2)$$

where τ_x is the zonal surface stress (available in the CMIP5 archive). (2) will form the basis of our analysis in subsection 3.2.

The generalized Ekman balance Equation (1) is a purely diagnostic relation for **U** that can be solved numerically when the pressure and tropospheric winds are supplied (Stevens et al. 2002). The need for relying on a numerical solution arises from the non-linear surface drag term represented by $-\mathbf{U} \parallel \mathbf{U} \parallel \frac{C_D}{h} = -\mathbf{U}\sqrt{U^2+V^2}\frac{C_D}{h}$. When this term is linearized as $-\mathbf{U}w_d/h$, where w_d is a constant, (1) can be solved analytically to yield (see BB09)

$$U = \frac{U_T\epsilon_i\epsilon_e + V_T f\epsilon_e - \alpha_0(f\partial p_s/\partial y + \epsilon_i \partial p_s/\partial x)}{\epsilon_i^2 + f^2} \quad (3a)$$

$$V = \frac{V_T\epsilon_i\epsilon_e - U_T f\epsilon_e + \alpha_0(f\partial p_s/\partial x - \epsilon_i \partial p_s/\partial y)}{\epsilon_i^2 + f^2} \quad (3b)$$

where $\epsilon_e = w_e/h$ and $\epsilon_i = (w_e + w_d)/h$. With U_T taken as the 850 hPa wind, $w_e/h \equiv 2\times10^{-5}s^{-1}$, and $w_d/h \equiv 1.5\times10^{-5}s^{-1}$ these analytic expressions reproduce the surface winds quite accurately. Using the ERA-40 reanalysis BB09 report a pattern correlation of 0.98 between the annual means of "modeled" and actual tropical surface winds. This success may seem unsurprising in view of the fact that the MLM prescribes surface pressure but as we shall see in section 3, the pressure term does not necessarily dominate this balance.

The surface pressure terms in (3) can be split into contributions from the PBL and free troposphere by writing $p_s = p_{FT} + p_{PBL}$, where p_{FT} is calculated as the pressure at the 1500m height level, and p_{PBL} as the residual from the known value of p_s. (The method is somewhat different from the one used by BB09 but essentially yields the same results). This decomposition can be substituted in to (3) to derive the relative contributions of the PBL and the free troposphere to the surface pressure gradient force.

The MLM contains some idealizations that may be problematic, such as constant ratios of entrainment velocity and drag coefficient over PBL thickness (w_e/h and w_d/h), and the use of winds from a constant pressure level for entrainment calculations, despite the fact that PBL thickness varies considerably over the tropical oceans. On the other hand, the MLM offers several advantages. First, it produces a fairly accurate representation of the surface winds using input that is readily available in the reanalysis data and CMIP5 archive. One could use more complex models to understand the influences on surface winds but these do not necessarily perform well in the region as evidenced by the relatively poor skill in the tropical Atlantic of the primitive equation model with prescribed heating employed by Chiang et al. (2001). The second reason for using the MLM is that it computes the actual velocity components rather than the tendency terms that one obtains from a momentum budget analysis. This facilitates the interpretation of the results. 3) Last, the MLM allows for a straightforward separation between PBL and free tropospheric contributions to the surface winds, as outlined above in this section. We therefore use this diagnostic tool to supplement our analysis.

3. Climatological mean winds in MAM

3.1. Surface pressure gradient

It is generally assumed that the zonal surface pressure gradient force is the main driver of the surface easterlies that prevail over the equatorial Pacific and Atlantic year round. Figure 1 shows that this is not the case in the equatorial Atlantic during boreal spring when the pressure gradient force is directed eastward from the African coast to 25ºW in ICOADS (pressure gradient approximately -9.7E-10 Pa/m) and to 30ºW (pressure gradient approximately -5.1E-10 Pa/m) in ERA-Int. Despite the eastward pressure gradient force the surface winds remain easterly during this season except for the far eastern equatorial Atlantic (orange line in Fig. 2a). In the GCMs the eastward pressure gradient force extends further west, almost to the South American coast (pressure gradient approximately -3.2E-10 Pa/m) but nevertheless surface winds are easterly in the ensemble mean (Fig. 2a), though in a few models the winds reverse (not shown).

The far eastern Pacific presents a similar picture with the eastward pressure gradient force extending up to about 40 degrees off-shore from the South American coast during MAM in the GCMs and ICOADS. In the ERA-Int, on the other hand, the Pacific pressure gradient is close to neutral. Despite the eastward (or neutral, in the case of ERA-Int) pressure gradient force the equatorial surface winds are directed westward in both observations and GCMs (not shown).

The zonal gradient of the equatorial surface pressure is largely consistent with that of the underlying SST (Fig. 1). This supports the assumption of the LN model concerning the relation of surface pressure and SST. On the other hand, as we have shown above, the LN model would fail to predict the MAM surface easterlies because it relies on surface pressure gradients only. It should be noted, however, that LN87 did not design their model to calculate the zonal mean but deviations from it, and that their model was initially intended for the subtropics, though it has informed many equatorial studies as well (e.g Jin 1997).

3.2. Surface momentum budget

To examine why the equatorial surface winds are easterly despite the opposing pressure gradient force we calculate the terms in the surface momentum budget (2). Here we focus on the climatological annual cycle averaged over the region 40°-10°W, 2°S-2°N (equatorial Atlantic wind or EAW index), in which the ocean is particularly sensitive to surface wind forcing (e.g. Richter et al. 2014). Figure 2a shows that the pressure gradient contribution is close to zero or positive (westerly) and therefore not able to balance the positive drag term. Rather this is accomplished by meridional advection and entrainment, with the latter term typically dominating in winter and spring. Meridional advection behaves quite similarly in all three datasets (ICOADS, ERA-Interim and GCM ensemble) in that it remains negative (easterly contribution) throughout the year, with the strongest contribution in boreal summer. Entrainment also remains negative throughout the year (because winds are stronger in the free troposphere than at the surface) but tends to be pronounced when meridional advection is weak and vice versa.

As an alternative measure of entrainment (or vertical mixing in general) we have computed the residual resulting from considering only advection, pressure gradient and surface drag in equation (2) and multiplied this quantity by minus one. This measure of vertical mixing agrees reasonably well with the parameterized entrainment in some months (January through May for ERA-Interim and April through August for the GCMs) but is too negative in others. This is particularly obvious in ERA-Interim during summer, when the residual suggests a positive contribution while entrainment remains negative (though small).

It is obvious that the choice of w_e and h in equation (2) has a crucial influence on the balance of terms. On the other hand, these parameters are not well constrained by observations, with estimates ranging from 1-2cm/s and 500-1500m for w_e and h, respectively (McGauley et al. 2004; de Szoeke et al. 2005; Ahlgrimm and Randall 2006; Chan and Wood 2013). For our calculations we chose w_e =1cm/s and h=1000m because these values lie within the range of observations and produce a small residual on the equator. We note that the resulting w_e/h is only half the value used by Stevens et al. 2002 and BB09. The entrainment term thus calculated should therefore be regarded a conservative estimate. Keeping in mind the uncertainties of the surface momentum budget, the above results nevertheless suggest that entrainment is essential in maintaining the surface easterlies on the equator.

3.3. Role of 850 hPa winds

Since the entrainment term solely depends on the 850 hPa wind we turn our attention to this field. A seasonally stratified correlation analysis of temporal variability in the EAW region (Fig. 3) shows that the 850 hPa and surface zonal winds are highly correlated, particularly in MAM, with a correlation coefficient higher than 0.9 in many GCMs and as high as 0.98 in the ERA-Int. During other seasons this correlation is lower but still remains above 0.6 in most datasets. One explanation for the high correlation in MAM is that the 850 hPa level is still inside the typically well-mixed PBL, in which case a higher level should be chosen to represent the free troposphere. Observations are sparse for the region, but a recent study by Chan and Wood (2013) using radio occultation data indicates that 850 hPa is just above the PBL top during MAM. The CMIP5 archive does not contain data on PBL depth so that we cannot assess its role in the models.

To analyze the factors controlling 850 hPa wind we perform an analysis of its momentum budget based on equation (2) but without the drag and entrainment terms and with the pressure gradient term replaced by the height gradient term $g\nabla_p Z$ (Fig. 2b). The residual in the reanalysis is relatively small from January through May, indicating that the balance between easterly contributions from the height gradient and westerly contributions from horizontal advection holds fairly well in these months. In other months the residual indicates that a westerly contribution is needed to close the balance. This might come from subgrid scale processes that are not available in the reanalysis data. We note that the height gradient at 850 hPa provides easterly momentum in March and April, which contrasts with the westerly contribution from the surface pressure gradient during these months (Fig. 2a). The reason for this is likely that the underlying SST has a stronger influence on sea-level pressure, as evidenced by Fig. 1.

3.4. MLM analysis

While the budget analysis suggests that entrainment is an important contribution to the surface wind balance it does not allow to quantify individual contributions. For this we turn to the MLM because it calculates contributions to the surface winds rather than tendencies. These contributions are: the zonal and meridional entrainment terms, and the zonal and meridional pressure gradient terms (Eq. 3). The sum of these terms compares reasonably well with the climatological MAM surface winds for both reanalysis (Fig. 4a) and GCMs (Fig. 4b). However, the MLM has a tendency to underestimate the easterlies in the equatorial belt and overestimate them in the subtropics (Fig. 4cd). Note that these errors are similar to those of typical GCMs relative to observations (see section 5). One reason for this westerly bias on the equator is that the MLM neglects advection, which contributes easterly momentum as we have seen in subsection 3.2. A way of reducing the error on the equator would be to increase the value of w_e/h in the MLM but this increases errors elsewhere.

Close to the equator, the two terms containing the Coriolis parameter are negligible, leaving the zonal entrainment and pressure gradient terms, whose seasonal evolution is shown in Fig. 5. The gradient term produces westerly winds in the central and eastern basin, consistent with our budget analysis (Fig. 2a). This term, however, is typically much weaker (in terms of magnitude) than the easterly contribution of the entrainment term in the central and western equatorial Atlantic. The pressure gradient term is negative during the rest of the year and, during boreal summer and fall, accounts for up to 50% of the easterlies in the western equatorial Atlantic. Overall the MLM analysis suggests that entrainment is crucial for maintaining surface easterlies on the equator. We note, however, that the values for the drag and entrainment coefficients (ε_e and ε_i) we use here where tuned to optimally reproduce the actual winds (Stevens et al. 2002). Since the MLM does not account for the easterly contribution from advection the entrainment may overcompensate for this missing process. Thus the entrainment term in the MLM likely represents a generous estimate of the actual entrainment contribution.

The high correlation between wind anomalies at the surface at and 850 hPa (Fig. 3) as well as the vertical wind profile (Fig. 11) hint at the possibility that the 850 hPa level is still inside the well-mixed PBL. We have therefore recalculated the MLM using 700 hPa as the separation between PBL and free troposphere but, in terms of the residuals, the results only marginally improve during MAM and significantly deteriorate during other parts of the year. It is also possible that the frequent occurrence of deep convection (the ITCZ is closest to the equator in MAM) renders the concept of a well-defined PBL top with steady entrainment unrealistic.

4. Interannual variability of equatorial winds

Surface winds over the equatorial Atlantic have their highest interannual variability during MAM (Fig. 8; Richter et al. 2012) and this strongly influences the zonal mode of equatorial Atlantic SST variability (Richter et al. 2014). Therefore our focus in this section will be on the factors controlling interannual variability of surface winds in MAM. The MLM reproduces fairly well the interannual variability of surface winds in the equatorial region with correlations typically exceeding 0.9 in both reanalysis and piControl GCMs (not shown). Using the EAW index as a criterion we composite the pressure gradient and entrainment terms in observations and piControl simulations (Fig. 6). The results show that, in the equatorial region, entrainment dominates over the pressure gradient. The latter term can be split into PBL and free tropospheric contributions (see section 2.3). The total free tropospheric contribution to surface wind variability can then be considered as the sum of entrainment and free tropospheric pressure gradient terms. Averaging over the EAW region one then obtains the result that free tropospheric processes constitute 84.5% of variability in the reanalysis and 92.1% in the GCMs. Since the MLM likely overestimates the entrainment contribution (see section 3.4) we repeated this analysis for the momentum budget terms (equation 2) and found that the free tropospheric contribution is 55.6% in the reanalysis and 62.8% in the GCMs. The momentum budget analysis further yields the advection contributions. These turn out to be almost one order of magnitude smaller than the pressure gradient and entrainment terms. Moreover the zonal and meridional advection terms are of opposite sign and therefore partially cancel. Thus the effect of horizontal advection seems negligible in the interannual variability of surface winds.

The above results suggest that surface wind variability is strongly influenced by the free tropospheric pressure distribution. The pressure distribution, in turn, should be closely linked to the patterns of deep convection. We examine this relation by compositing precipitation and surface pressure based on the EAW index (Fig. 7a). The precipitation anomalies are confined in an equatorial band between 10ºS-10ºN with dry anomalies north and wet anomalies south of the equator (see also Richter et al. 2014). The dry precipitation pole is associated with high-pressure anomalies in the same region and to the northwest. The wet pole, on the other hand, is associated with low-pressure anomalies to the southeast, though this is less clear in the ERA-Int. The subtropical pressure anomalies are indicative of a westward shift of the North Atlantic anticyclone and a southwestward shift of the South Atlantic anticyclone (Fig. 7b). These features (all significant at the 95% level; not shown) suggest that equatorial surface wind variability is associated with subtropical anomalies though it is not clear whether there exists a causal link. A lagged correlation analysis of daily mean EAW surface winds and sea-level pressure in the subtropical South Atlantic (30W-0, 15-5S) indicates that correlation is highest when the pressure leads by 1-7 days, depending on the model (not shown). This is consistent with subtropical influences on the equatorial surface winds but more work will be needed to establish causality. We note that the South Atlantic influence is consistent with the results of Richter et al. (2010) and Luebbecke et al. (2010), who showed that a weakening of the South Atlantic high often precedes warm anomalies in the equatorial Atlantic and Benguela upwelling regions.

The surface pressure anomalies can be split into contributions from the PBL and the free troposphere (see section 2) and this analysis suggests that both terms contribute equally and have similar structure (not shown). Thus there does not appear to be a clear separation between PBL and free tropospheric contributions to surface pressure anomalies in MAM. This is consistent, to some extent, with the results of Chiang et al. (2001) and BB09, who found that PBL and free tropospheric contributions to surface pressure are important to zonal surface winds. To further examine the influence of SST on equatorial winds we compare the variability of MAM surface winds in experiment piControl with that of sstClim. Since in the latter experiment each GCM is forced with its climatological SSTs, the contribution from anomalous SST gradients is excluded by design. Due to the fact that the sstClim simulations are typically only 30 years long, as opposed to 500-1000 years in piControl, we calculated the variance of the piControl simulations over successive 30-year windows and averaged over the results.

The MAM variance of the surface zonal wind decreases by approximately 22% in sstClim relative to piControl in the ensemble mean (Table 2). Individual GCMs vary considerably, with the relative changes ranging from -82% (HadGEM2-A) to +110% (MPI-ESM-MR). Notwithstanding the intermodel spread, the results suggest that a significant portion of MAM equatorial surface wind variability cannot be explained by SST anomalies. Importantly, even with prescribed climatological SST the maximum variability of equatorial zonal surface winds occurs in May (Fig. 8). This suggests that the seasonality of wind variability is dominated by internal atmospheric variability rather than by local or remote SST anomalies.

To further investigate the atmospheric processes behind the equatorial Atlantic surface wind anomalies, we use the EAW index to composite sea-level pressure (SLP), surface winds, and precipitation anomalies in the sstClim models. Due to the relatively short integration time of sstClim (typically 30 years) the significance of the results is difficult to establish. Keeping this caveat in mind we examine the composites (Fig. 9). In addition to the zonal SLP dipole that drives westerly surface wind anomalies on the equator, we also note low pressure over North and Northwest Africa, and a weakening of the South Atlantic high. The precipitation response is limited to the equatorial Atlantic region with the familiar southeastward shift of deep convection (Richter et al. 2014). Note that the composite patterns of precipitation and SLP are very similar to those obtained from the fully coupled simulations over the equatorial Atlantic. This suggests that internal variability plays a dominant role in shaping the patterns of co-variability among equatorial surface wind, sea-level pressure and precipitation.

The notion that deep convection is strongly controlled by the underlying SST has formed the basis of many simple and intermediate models of convection (e.g. Emanuel et al. 1994, Sobel and Bretherton 2000). The general idea is that warm SSTs destabilize the overlying atmosphere and that therefore deep convection roughly follows the location of the warmest SST. The climatological MAM SST distribution in the tropical Atlantic, however, is relatively uniform and shows no correspondence with the underlying SST (Fig. 10). In the absence of local constraints, the location of deep convection may be susceptible to remote influences, such as the interhemispheric SST gradient (see Xie and Carton 2004 and references therein) or atmospheric internal variability as suggested by the climSST results.

5. On the westerly surface wind bias in GCMs

Both coupled ocean-atmosphere and stand-alone atmospheric GCMs are subject to persistent westerly wind biases over the equatorial Atlantic (see Richter et al. 2014 for an evaluation of CMIP5 models). Keeping in mind its limitations, we revisit the

MLM results (section 3.4) as the starting point of our discussion. Despite the MLM's tendency to underestimate the strength of the equatorial easterlies in GCMs its results are still representative of the actual GCM biases (relative to ERA-Int). For the EAW index region, the MLM results for the GCM piControl ensemble have a zonal wind bias of 1.4 m/s relative to ERA-Int in MAM. Of this bias, 62% is due to the entrainment term, with the remaining 38% due to the pressure gradient term. Splitting the pressure gradient term into PBL and free tropospheric contributions shows that both are about equally important with the former 53% and the latter 47%. Thus the combined influence of free tropospheric conditions (entrainment and pressure gradient) accounts for about 80% of the bias. The erroneously weak entrainment term in GCMs (relative to ERA-Int) has to be due to a westerly bias in the 850 hPa winds because the entrainment velocity w_e is constant in the MLM calculations. The momentum budget analysis for the EAW region at 850 hPa (Fig. 2b) shows that the easterly contribution of meridional advection is comparable in ERA-Int and GCMs, which suggest that meridional advection, while important to the momentum balance, is not the main reason for the model biases. A striking difference between ERA-Int and the GCMs is that the geopotential height gradient term in MAM is large and positive in the GCMs but small and negative in the reanalysis. This suggests that errors in the geopotential height gradient play a large role in the westerly bias at 850 hPa.

A longitude-height section of the zonal height gradient term in GCMs (Fig. 11b) shows westerly acceleration over the whole width of the equatorial Atlantic and up to a height of 500 hPa in MAM. This contrasts with the ERA-Int (Fig. 11a), where the term contributes easterly acceleration over the western equatorial Atlantic and extends further to the east with height. The westerly contribution from the height gradient term in GCMs is consistent with the fact that the models generate deep convection mostly south of the equator during MAM, resulting in relatively high pressure on the equator (Richter and Xie 2008, Richter et al 2014). In the reanalysis, on the other hand, deep convection mostly occurs over equatorial South America and the western equatorial Atlantic, leading to relatively low pressure there. The spurious southward excursion of the simulated ITCZ may also explain the excessively large seasonal cycle of the height gradient term in GCMs due to the close link between pressure and deep convection.

The geopotential height gradient term at 850 hPa in MAM in the GCMs (Fig. 2b) is not balanced by either horizontal or vertical advection, leaving a large residual. It is not clear which process supplies the missing momentum. Analysis of daily means suggests that transient advection does not play an important role. Another possibility is convective momentum transport or other parameterized processes. Since these terms are not available from the CMIP archive, simulations that output all the terms in the momentum equation would be needed to quantify the importance of such processes in GCMs. The more important question, however, is how these processes compare to the real world. This is beyond the scope of the present study and will be left to future work.

6. Summary and conclusions

We have investigated the factors influencing the surface winds over the equatorial Atlantic. Our results show that during MAM the surface pressure gradient force is directed eastward over the central and eastern basin in both observations and GCMs. Thus other processes must act to maintain easterly winds during this season. The surface momentum budget suggests that PBL entrainment and meridional advection are important contributors of easterly momentum. A simple diagnostic model of the surface winds (Stevens et al. 2002) further emphasizes the importance of entrainment.

Neither method takes account of convective momentum transport, which might play an important role during MAM, when deep convection often occurs over the equatorial Atlantic. Strong vertical mixing is also suggested by the high correspondence between surface and 850 hPa zonal winds.

Interannual variability of the equatorial zonal surface winds in MAM is, according to the MLM analysis, dominated by free tropospheric processes, namely PBL entrainment and the contribution of the free troposphere to the surface pressure gradient. These terms contribute roughly 90% of the variability in both reanalysis and GCMs. A similar analysis based on the surface momentum budget estimates the free tropospheric contribution at 56% and 63% for reanalysis and GCMs, respectively. Both analyses suggest that a large portion of MAM zonal surface wind variability is due to free tropospheric contributions rather than the underlying SST and associated pressure gradients. This is also supported by the fact that the simulated variability of zonal surface winds is reduced by only 22% when climatological SSTs are prescribed. Composite analysis shows that westerly equatorial wind anomalies are associated with a southeastward shift of deep convection. The associated surface pressure anomalies are consistent with the westerly wind anomalies.

Previous results have shown that surface wind anomalies, particularly during MAM, have a crucial influence on the development of Atlantic Niños (Servain et al. 1982; Zebiak 1993; Keenlyside and Latif 2007; Richter et al 2014). If these surface wind anomalies are largely due to internal atmospheric variability, as suggested by our analysis, then this greatly diminishes the prospects of skillful prediction of Atlantic Niños. This pessimistic view is consistent with the low skill of current prediction systems (Stockdale et al. 2006), the insufficient strength of coupled feedbacks (Zebiak 1993), and the apparent lack of consistent remote influences from the Pacific (Chang et al. 2006). Nevertheless, the slow oceanic response to surface wind forcing should permit skillful predictions at least a few months ahead.

According to our results (and those of Richter et al. 2014) surface wind and precipitation anomalies are closely linked. Precipitation, in turn, is often assumed to closely follow the underlying SST and thus one might expect that the surface wind anomalies ultimately result from SST anomalies. Our analysis of GCMs with prescribed climatological SSTs, however, suggests that this is not the case because pronounced surface wind anomalies develop even in the absence of SST anomalies.

While meridional advection of zonal momentum is an important component of the zonal wind budget, our results suggest that it cannot explain the equatorial westerly wind bias common to most GCMs. Rather our results indicate that it is the erroneous eastward pressure gradient force that lies at the heart of the problem. This eastward pressure gradient force is not confined to the surface but extends upward to about 500 hPa. As a result it not only weakens the surface winds but also the free tropospheric winds, which are mixed into the PBL and most likely are the major source of easterly momentum in observations. The lower tropospheric eastward pressure gradient force in GCMs is a consequence of the erroneous high pressure over the western equatorial Atlantic (relative to observations). Our results thus further support the hypothesis that errors in deep convection, particularly the dry bias over the western equatorial Atlantic and the Amazon, are a major contribution to the westerly wind bias (Chang et al. 2007, 2008; Richter et al 2008; Wahl et al. 2009; Tozuka et al. 2011; Richter et al. 2012; Zermeno and Zhang 2013; Richter et al. 2014).

In the introduction we posed the question whether surface winds are governed by SST gradients (Lindzen-Nigam paradigm) or mid-tropospheric heating (Gill paradigm). Our results indicate that SST and associated surface pressure gradients do not dominate the behavior of the equatorial Atlantic surface winds in MAM; neither their climatological mean nor their interannual variability. Thus the LN model, with its emphasis on SST and surface pressure gradients, has little explanatory power for this particular region and season. The Gill paradigm, on the other hand, considers mid-tropospheric processes and is therefore more relevant. This might be due to the fact that SST gradients are weak in the equatorial Atlantic during MAM, allowing other influences to dominate. It might be worthwhile to explore to what extent such conditions also exist in other tropical regions, such as the eastern equatorial Pacific in MAM.

Acknowledgments

The authors thank the three anonymous reviewers for their constructive comments. We acknowledge the World Climate Research Programme's Working Group on Coupled Modelling, which is responsible for CMIP, the U.S. Department of Energy's Program for Climate Model Diagnosis and Intercomparison which provides coordinating support and led development of software infrastructure for CMIP, and the climate modeling groups for making available their model output.

References

Adler RF, Huffman GJ, Chang A, Ferraro R, Xie P, Janowiak J, Rudolf B, Schneider U, Curtis S, Bolvin D, Gruber A, Susskind J, Arkin P (2003) The Version 2 Global Precipitation Climatology Project (GPCP) Monthly Precipitation Analysis (1979-Present). J. Hydrometeor 4:1147-1167

Ahlgrimm M, Randall D (2006) Diagnosing monthly mean boundary layer properties from reanalysis data using a bulk boundary layer model. J Atmos Sci 63:998–1012

Alexander MA, Bladé I, Newman M, Lanzante JR, Lau N-C, Scott JD (2002) The atmospheric bridge: the influence of ENSO teleconnections on air-sea interaction over the global oceans. J Clim 15: 2205–2231

Back LE, Bretherthon CS (2009a) On the relationship between SST gradients, boundary layer winds and convergence over the tropical oceans. J Clim 22:4182–4196

Back LE, Bretherton CS (2009b) A simple model of climatological rainfall and vertical motion patterns over the tropical oceans. J Clim 22:6477–6497

Bjerknes J (1969) Atmospheric teleconnections from the equatorial Pacific. Mon Weather Rev 97:163-172

Chan KM, Wood R (2013) The seasonal cycle of planetary boundary layer depth determined using COSMIC radio occultation data. J Geophys Res 118:12422-12434

Chang P, Fang Y, Saravanan R, Ji L, Seidel H (2006) The cause of the fragile relationship between the Pacific El Niño and the Atlantic Niño. Nature 443:324-328

Chang CY, Carton JA, Grodsky SA, Nigam S (2007) Seasonal climate of the tropical Atlantic sector in the NCAR Community Climate System Model 3: error structure and probable causes of errors. J Clim 20:1053–1070

Chang CY, Nigam S, Carton JA (2008) Origin of the springtime westerly bias in equatorial Atlantic surface winds in the Community Atmosphere Model version 3 (CAM3) simulation. J Clim 21:4766-4778

Chelton DB, Coauthors (2001) Observations of coupling between surface wind stress and sea surface temperature in the eastern tropical Pacific. J Climate 14:1479–1498

Chiang JCH, Zebiak SE, Cane MA (2001) Relative roles of elevated heating and surface temperature gradients in driving anomalous surface winds over tropical oceans. J Atmos Sci 58:1371-1394

Davey MK, Coauthors (2002) STOIC: a study of coupled model climatology and variability in topical ocean regions. Clim Dyn 18:403-420

Dee DP, Coauthors (2011) The ERA-Interim reanalysis: configuration and performance of the data assimilation system. Quart J R Meteorol Soc 137:553-597

Deser C (1993) Diagnosis of the surface momentum balance over the tropical Pacific Ocean. J Clim 6:64-74

deSzoeke SP, Bretherton CS, Bond NA, Cronin MF, Morely BM (2005) EPIC 95°W observations of the eastern Pacific atmospheric boundary layer from the cold tongue to the ITCZ. J Atmos Sci 62(2):426

Dunbar S, Coauthors (2006) QuikSCAT science data product user manual, version 3.0, Doc. D-18053—Rev A, Jet Propul. Lab., Pasadena, Calif. Available at ftp://podaac-ftp.jpl.nasa.gov/allData/quikscat/L2B/docs/QSUG_v3.pdf.

Emanuel KA, Neelin JD, Bretherton CS (1994) On large-scale circulations in convecting atmospheres. Quart J Roy Met Soc 120:1111-1143

Foltz GR, McPhaden MJ (2010) Abrupt equatorial wave-induced cooling of the Atlantic cold tongue in 2009. Geophys Res Lett 37, L24605, doi:10.1029/2010GL045522.

Gill AE (1980) Some simple solutions for heat-induced tropical circulation. Q J R Meteorol Soc 106:447–462

Jin F-F (1997) An equatorial ocean recharge paradigm for ENSO. Part I: Conceptual model. J Atmos Sci 54:811–829

Keenlyside NS, Latif M (2007) Understanding equatorial Atlantic interannual variability. J Clim 20:131-142

Lindzen RS, Nigam S (1987) On the role of the sea surface temperature gradients in forcing the low-level winds and convergence in the tropics. J Atmos Sci 44:2418–2436

Lübbecke JF, Böning CW, Keenlyside N, Xie S-P (2010) On the connection between Benguela and equatorial Atlantic Niños and the role of the South Atlantic anticyclone. J Geophys Res 115, C09015, doi:10.1029/2009JC005964

Lübbecke JF, McPhaden MJ (2012) On the Inconsistent Relationship between Pacific and Atlantic Niños. J Climate 25:4294–4303

McGauley M, Zhang C, Bond N (2004) Large-scale characteristics of the atmospheric boundary layer in the Eastern Pacific cold tongue-ITCZ region. J Clim 17:3907-3920

Neelin JD, Battisti DS, Hirst AC, Jin FF, Wakata Y, Yamagata T, Zebiak S (1998) ENSO theory. J Geophys Res 103:14261–14290

Okumura Y, Xie S-P (2004) Interaction of the Atlantic equatorial cold tongue and African monsoon. J Clim 17:3588–3601

Philander SG (1990) El Niño, La Niña, and the Southern Oscillation. International Geophysics Series, 46, Academic Press Inc.

Richter I, Xie S-P (2008) On the origin of equatorial Atlantic biases in coupled general circulation models. Clim Dyn 31:587-598

Richter I, Behera SK, Masumoto Y, Taguchi B, Komori N, Yamagata T (2010) On the triggering of Benguela Niños: Remote equatorial versus local influences. Geophys Res Lett 37(L20604). doi:10.1029/2010GL044461

Richter I, Xie S-P, Wittenberg AT, Masumoto Y (2012) Tropical Atlantic biases and their relation to surface wind stress and terrestrial precipitation. Clim Dyn 38:985-1001. doi: 10.1007/s00382-011-1038-9.

Richter I, Behera SK, Masumoto Y, Taguchi B, Sasaki H, Yamagata T (2013) Multiple causes of interannual sea surface temperature variability in the equatorial Atlantic Ocean. Nature Geosci 6:43-47

Richter I, Xie S-P, Behera SK, Doi T, Masumoto Y (2014) Equatorial Atlantic variability and its relation to mean state biases in CMIP5. Clim Dyn 42:171-188, doi: 10.1007/s00382-012-1624-5

Servain J, Picaut J, Merle J (1982) Evidence of remote forcing in the equatorial Atlantic Ocean. J Phys Oceanogr 12:457–463

Sobel AH, Bretherton CS (2000) Modeling tropical precipitation in a single column. J Clim 13:4378-4392

Stevens B, Duan JJ, McWilliams JC, Münnich M, Neelin JD (2002) Entrainment, Rayleigh friction, and boundary layer winds over the tropical Pacific. J Clim 15:30–44

Stockdale TN, Balmaseda MA, Vidard A (2006) Tropical Atlantic SST prediction with coupled ocean-atmosphere GCMs. J Clim 19:6047-6061

Tozuka T, Doi T, Miyasaka T, Keenlyside N, Yamagata T (2011) Key factors in simulating the equatorial Atlantic zonal sea surface temperature gradient in a coupled general circulation model. J Geophys Res 116(C06010), doi:10.1029/2010JC006717

Wahl S, Latif M, Park W, Keenlyside N (2009) On the Tropical Atlantic SST warm bias in the Kiel Climate Model. Clim Dyn, DOI 10.1007/s00382-009-0690-9

Wallace JM, Mitchell TP, Deser C (1989) The influence of sea-surface temperature on surface wind in the Eastern Equatorial Pacific: Seasonal and interannual variability. J Climate 2:1492-1499.

Wallace JM, Smith C, Bretherton CS (1992) Singular value de- composition of wintertime sea surface temperature and 500-mb height anomalies. J Clim 5: 561–576

Woodruff SD, Coauthors (2011) ICOADS Release 2.5: Extensions and enhancements to the surface marine meteorological archive. Int J Climatol 31:951-967

Xie S-P (2004) Satellite observations of cool ocean–atmosphere interaction. Bull. Amer. Meteor Soc 85:195–208

Xie S-P, Carton JA (2004) Tropical Atlantic variability: Patterns, mechanisms, and impacts. In *Earth Climate: The Ocean-Atmosphere Interaction*, C. Wang, S.-P. Xie and J.A. Carton (eds.), Geophysical Monograph, 147, AGU, Washington D.C., 121-142.

Zebiak SE (1993) Air–sea interaction in the equatorial Atlantic region. J Clim 6:1567–1586

Zermeno D, Zhang C (2013) Possible Root Causes of the Surface Westerly Biases over the Equatorial Atlantic in Global Climate Models. J Clim, in press

Captions

Table 1. List of the 12 GCMs analyzed in this study. The same set of GCMs is used for analysis of two different experiments: piControl (control experiment with fully coupled GCMs and pre-industrial greenhouse gas forcing) and sstClim (GCMs forced with SST climatology of their coupled control experiment. The CAN-ESM2 and HadGEM2-ES piControl runs have no exact counterpart in the other two experiments, so he nearest equivalents (Can-AM4 and HadGEM2-A) are chosen.

Table 2. Standard deviation (m/s) of EAW zonal wind in MAM for experiments piControl (second column) and sstClim (third column). The rightmost column shows the relative change of the standard deviation in experiment sstClim. Each row shows the results for one particular GCM, with the bottom row showing the ensemble average.

Fig. 1. SLP (in hPa; solid lines) and SST (in C; dashed lines) along the equator averaged from 2°S-2°N and over MAM for **a** the Atlantic basin, and **b** the Pacific basin. Black denotes ICOADS observations, green the ERA-Interim reanalysis, and blue the ensemble mean of piControl GCMs.

Fig. 2. Climatological annual cycle of the zonal momentum budget for the EAW region (40-10ºW, 2ºS-2ºN) at **a** the surface and **b** the 850 hPa level. The top row shows ICOADS observations (surface only), the middle row shows the ERA-Interim reanalysis, and the bottom row shows the piControl ensemble mean. The individual colors denote pressure gradient (green; geopotential height gradient at the 850 hPa

level), meridional advection (blue), surface drag (orange; surface only), PBL entrainment (red; surface only), horizontal advection (purple; 850 hPa only), and the residual (brown). The residual is calculated as the sum of the pressure gradient, horizontal advection and surface drag terms minus the actual wind tendency and multiplied by minus one.

Fig. 3. Seasonally stratified correlation of EAW surface and 850 hPa zonal winds for the ERA-Interim reanalysis and the members of the piControl ensemble.

Fig. 4. **a,b** MAM surface zonal winds calculated with the MLM equations (shading; units m/s) and the actual surface winds (contours; units m/s; contour interval 1 m/s; negative contours dashed). **c,d** Error of MLM surface winds relative to the actual winds (m/s) in MAM. The left column shows the ERA-Interim reanalysis, the left column the piControl ensemble mean.

Fig. 5. Hovmoeller plot of Entrainment term (shading; m/s) and pressure gradient term (contours; interval 0.5 m/s) averaged along the equator from 2°S-2°N for **a** ERA-Interim, and **b** piControl ensemble.

Fig. 6. Anomalous entrainment term (shading; m/s) and pressure gradient term (contours; interval 0.25 m/s) composited on the EAW zonal wind index for **a** ERA-Interim, and **b** the piControl ensemble. The criterion for compositing is +2 standard deviations. Only maxima occurring in MAM are considered.

Fig. 7. Precipitation and sea-level pressure fields for the ERA-Interim reanalysis (top row) and the piControl GCM ensemble (bottom row). **a** Precipitation (shading; mm/d) and sea-level pressure (contours; interval 0.1 hPa) anomalies composited on 2 standard deviations of the EAW zonal wind index. **b** Climatological MAM precipitation (shading; mm/d) and sea-level pressure (contours; interval 1 hPa).

Fig. 8. Variance of zonal winds (m^2/s^2) in the EAW region stratified by month for the ERA-Interim reanalysis (solid black line), the piControl ensemble (solid blue line), and the sstClim ensemble (dashed blue line) in which GCMs are forced with their respective SST climatologies.

Fig. 9. Anomalous sea-level pressure (shading; hPa), precipitation (contours; interval 0.5 mm/d), and surface winds (vectors; reference 1 m/s) composited on +2 standard deviations the EAW zonal wind index. The figure shows the ensemble average over sstClim GCMs. The analysis is restricted to MAM.

Fig. 10. MAM climatological precipitation (shading; mm/day) and SST (contours; interval 0.5 ºC; contours below 27 ºC are omitted) for **a** AVHRR SST and GPCP precipitation, **b** ERA-Interim reanalysis, and **c** the piControl GCM ensemble.

Fig. 11. Longitude-height section of the geopotential height gradient term in the momentum budget (shading; m/s/day), and zonal velocity (contours; intveral 1 m/s) for **a** the ERA-Interim reanalysis, and **b** the piControl ensemble. The fields represent the climatological MAM mean. Negative values of the gradient term correspond to easterly acceleration.

A. Tables

Model Name	Institution	Length of Simulation (years)
bcc-csm1-1	Beijing Climate Center, Beijing, China	500
BNU-ESM	Beijing Normal University, Beijing, China	559
CanESM2	Canadian Centre for Climate Modeling and Analysis, BC, Canada	996
CCSM4	National Center for Atmospheric Research, Boulder, CO, USA	501
FGOALS-s2	LASG, Beijing, China	501
GFDL-CM3	Geophysical Fluidy Dynamics Laboratory, Princeton, NJ, USA	500
HadGEM2-ES	Met Office Hadley Centre, Exeter, UK	575
inmcm4	Institute of Numerical Mathematics, Moscow, Russia	500
MIROC5	Atmosphere and Ocean Research Institute, Tokyo University, Japan	670
MPI-ESM-LR	Max Planck Institute for Meteorology, Hamburg, Germany	1000
MRI-CGCM3	Meteorological Research Institute, Tsukuba, Japan	500
NorESM1-M	Bjerknes Centre for Climate Research, Bergen, Norway	501

Table 1. List of the 12 GCMs analyzed in this study. The same set of GCMs is used for analysis of two different experiments: piControl (control experiment with fully coupled GCMs and pre-industrial greenhouse gas forcing) and sstClim (GCMs forced with SST climatology of their coupled control experiment). The CAN-ESM2 and HadGEM2-ES piControl runs have no exact counterpart in the other two experiments, so he nearest equivalents (Can-AM4 and HadGEM2-A) are chosen.

Model Name	Variance of EAW wind in MAM		% change relative to piControl
	piControl	sstClim	
bcc-csm1-1	1.70	1.69	-0.36
BNU-ESM	0.79	0.51	-35.4
CanESM2	1.16	0.55	-52.9
CCSM4	1.37	0.35	-74.7
FGOALS-s2	1.45	0.73	-49.8
GFDL-CM3	1.93	1.40	-27.2
HadGEM2-ES	2.54	0.45	-82.1
inmcm4	0.56	0.52	-8.2
MIROC5	2.28	1.86	-18.4
MPI-ESM-MR	1.14	2.41	+109.7
MRI-CGCM3	0.80	0.44	-45.3
NorESM1-M	1.98	2.49	+25.8
ensemble mean	1.16	1.48	-21.6

Table 2. Standard deviation (m/s) of EAW zonal wind in MAM for experiments piControl (second column) and sstClim (third column). The rightmost column shows the relative change of the standard deviation in experiment sstClim. Each row shows the results for one particular GCM, with the bottom row showing the ensemble average.

B. Figures

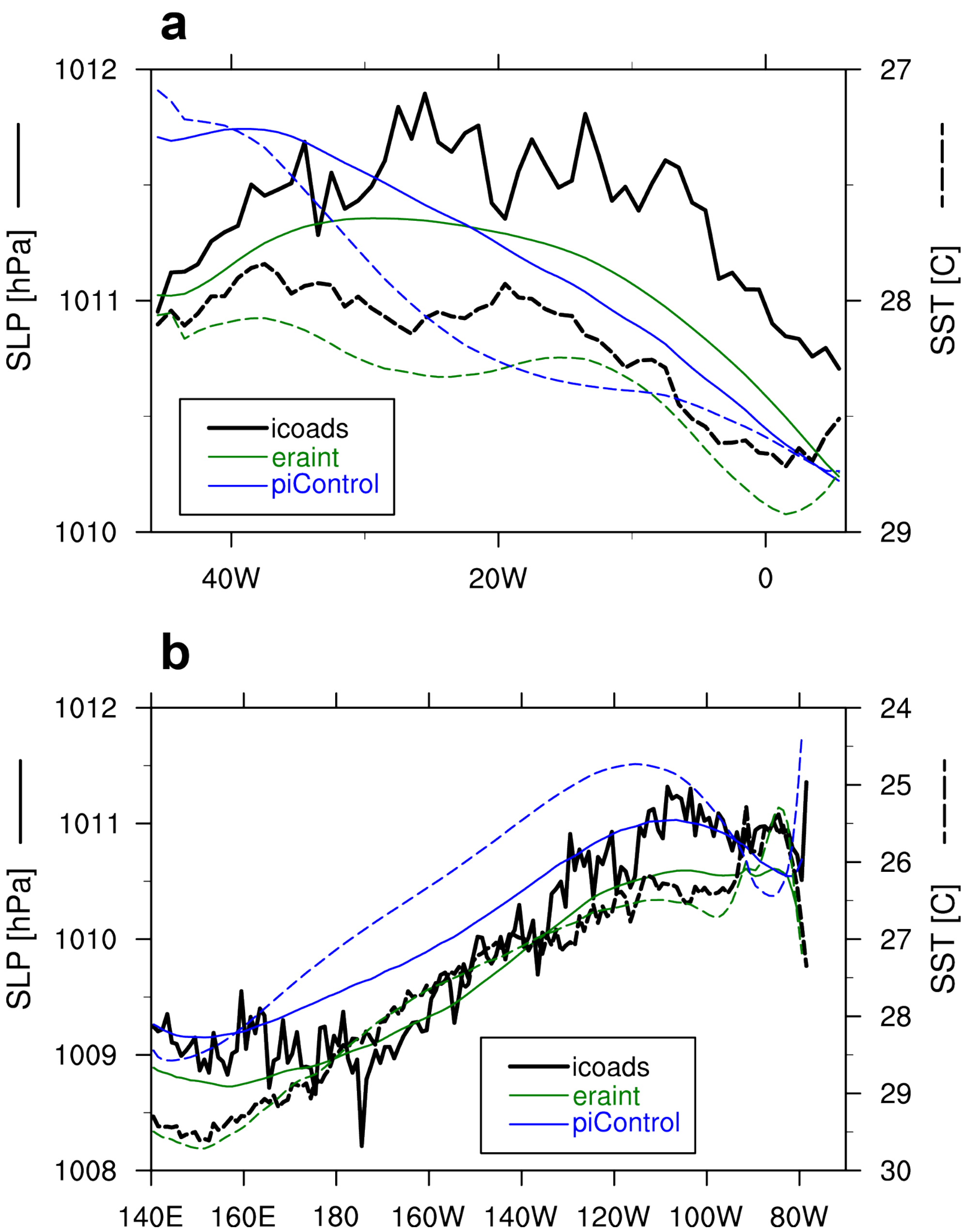

Fig. 1. SLP (in hPa; solid lines) and SST (in C; dashed lines) along the equator averaged from 2°S-2°N and over MAM for **a** the Atlantic basin, and **b** the Pacific basin. Black denotes ICOADS observations, green the ERA-Interim reanalysis, and blue the ensemble mean of piControl GCMs.

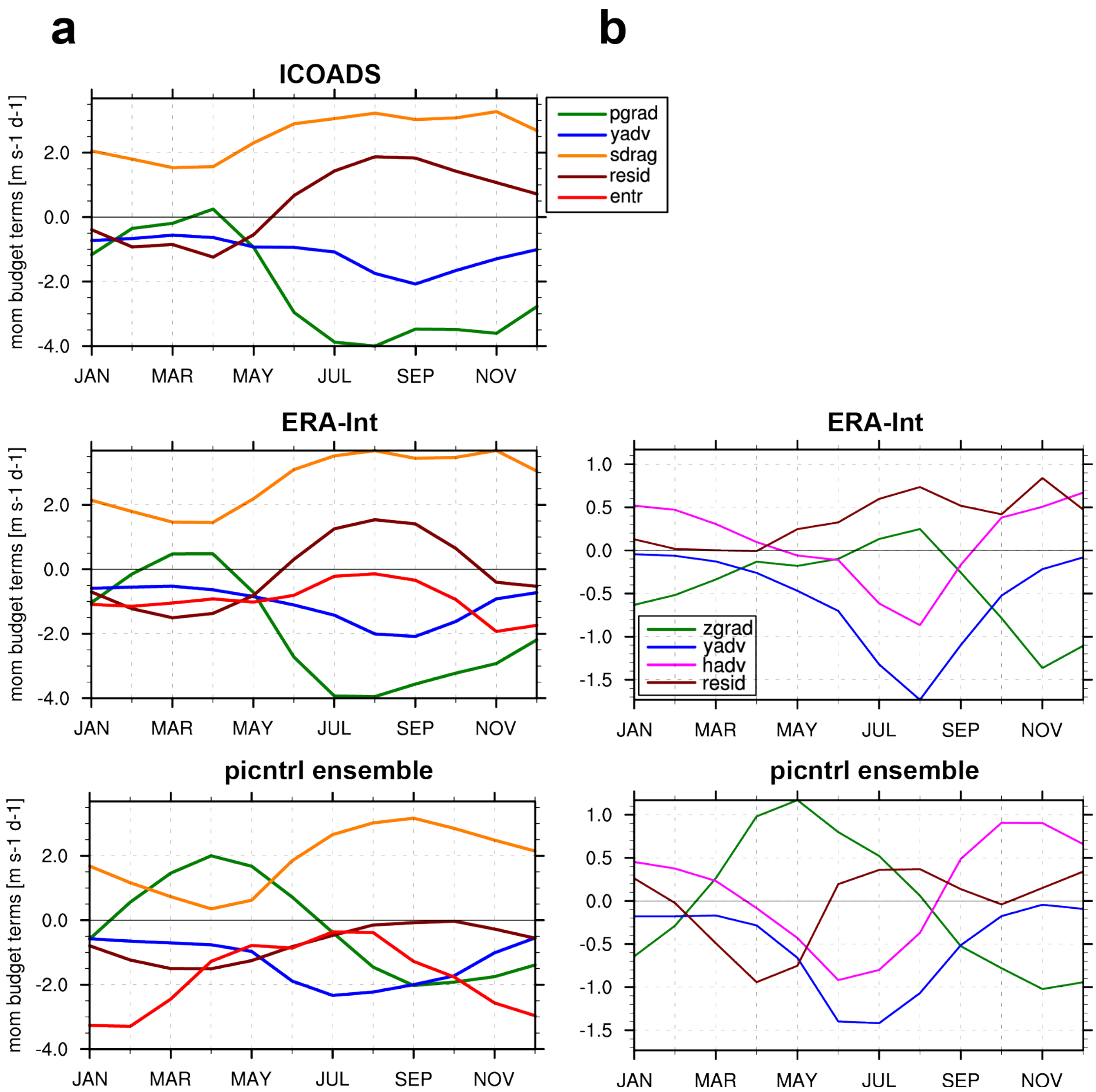

Fig. 2. Climatological annual cycle of the zonal momentum budget for the EAW region (40-10ºW, 2ºS-2ºN) at **a** the surface and **b** the 850 hPa level. The top row shows ICOADS observations (surface only), the middle row shows the ERA-Interim reanalysis, and the bottom row shows the piControl ensemble mean. The individual colors denote pressure gradient (green; geopotential height gradient at the 850 hPa level), meridional advection (blue), surface drag (orange; surface only), PBL entrainment (red; surface only), horizontal advection (purple; 850 hPa only), and the residual (brown). The residual is calculated as the sum of the pressure gradient, horizontal advection and surface drag terms minus the actual wind tendency and multiplied by minus one.

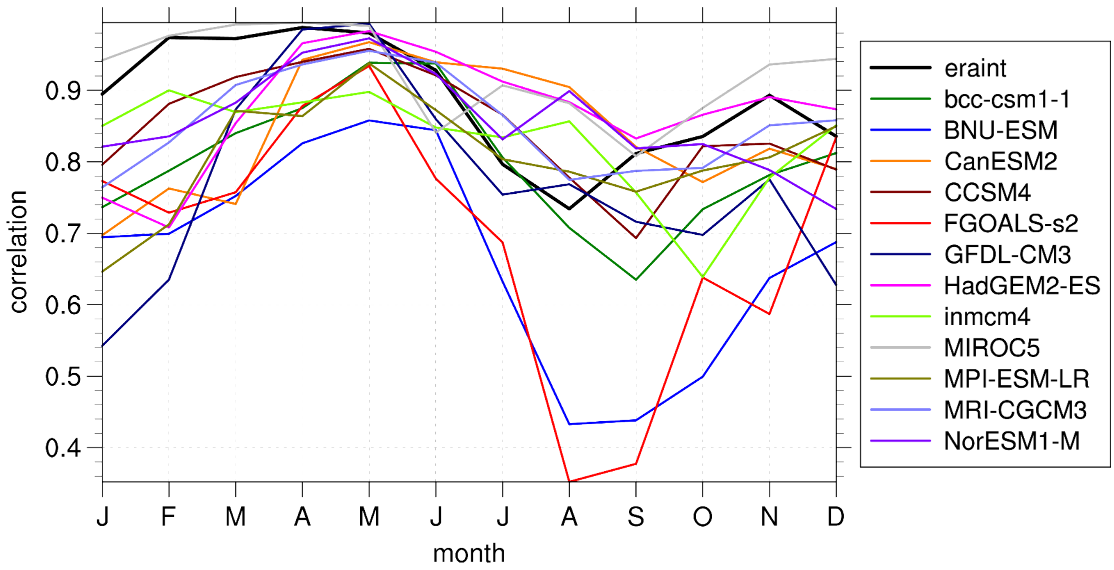

Fig. 3. Seasonally stratified correlation of EAW surface and 850 hPa zonal winds for the ERA-Interim reanalysis and the members of the piControl ensemble.

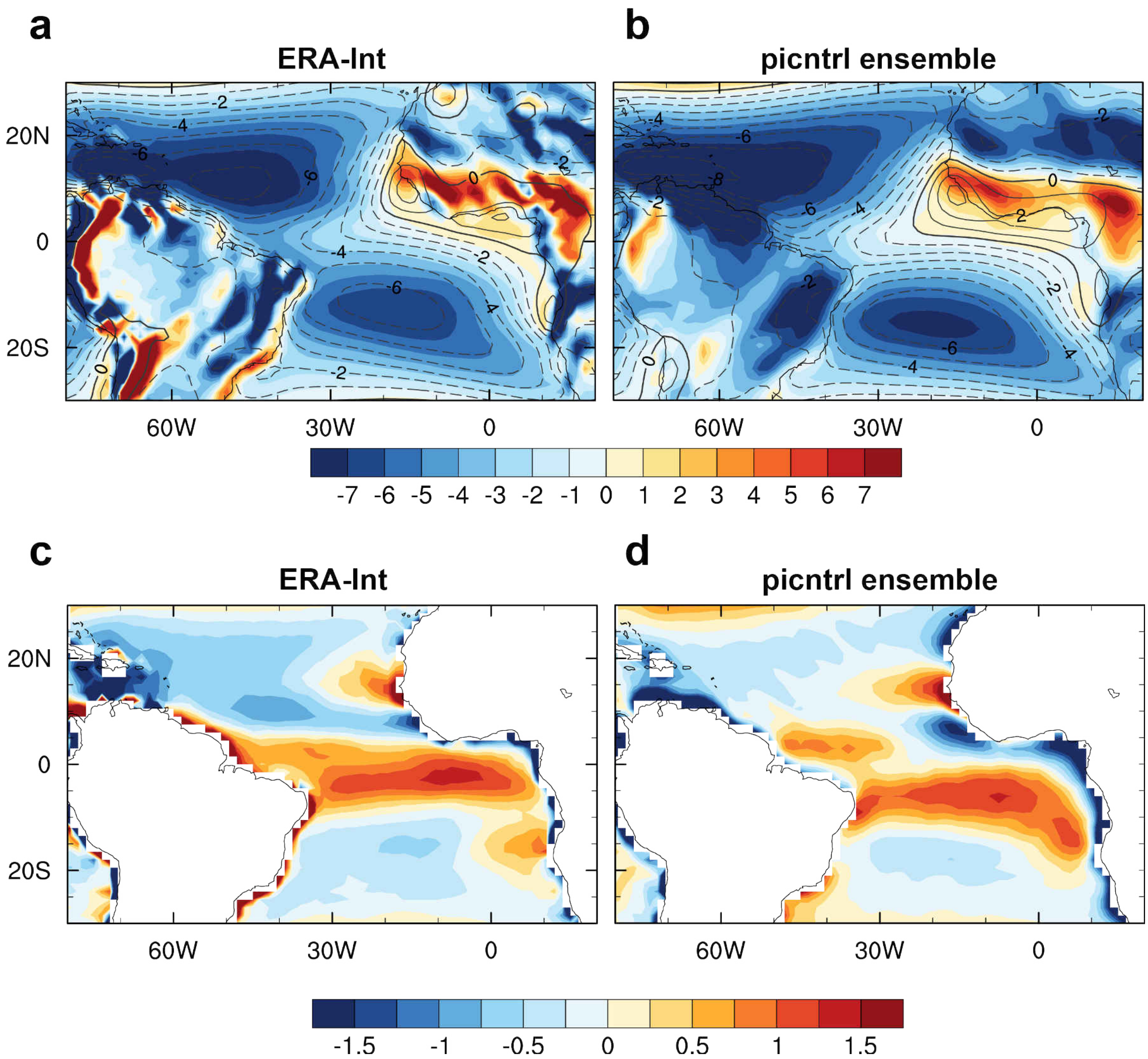

Fig. 4. **a,b** MAM surface zonal winds calculated with the MLM equations (shading; units m/s) and the actual surface winds (contours; units m/s; contour interval 1 m/s; negative contours dashed). **c,d** Error of MLM surface winds relative to the actual winds (m/s) in MAM. The left column shows the ERA-Interim reanalysis, the left column the piControl ensemble mean.

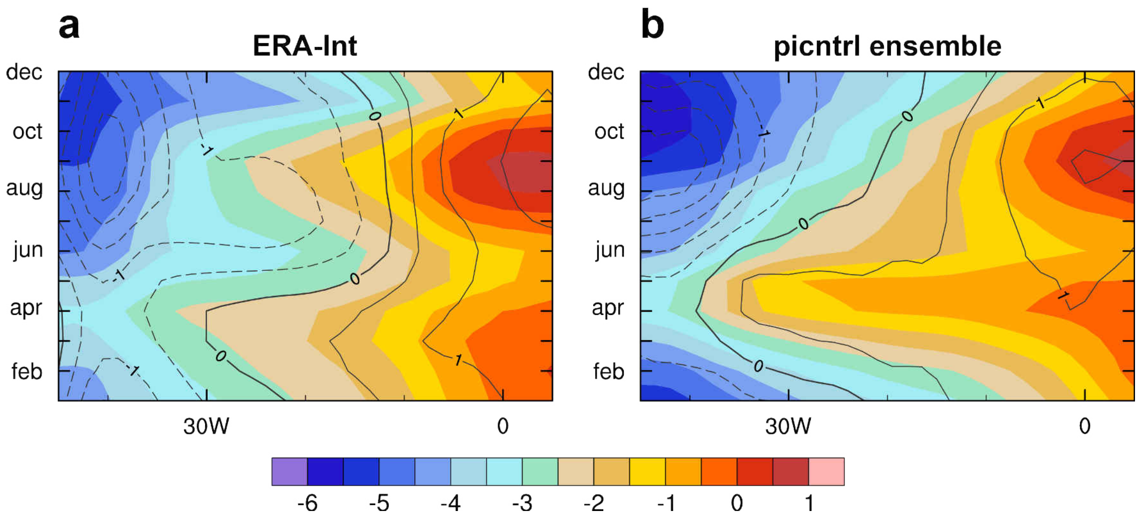

Fig. 5. Hovmoeller plot of Entrainment term (shading; m/s) and pressure gradient term (contours; interval 0.5 m/s) averaged along the equator from 2°S-2°N for **a** ERA-Interim, and **b** piControl ensemble.

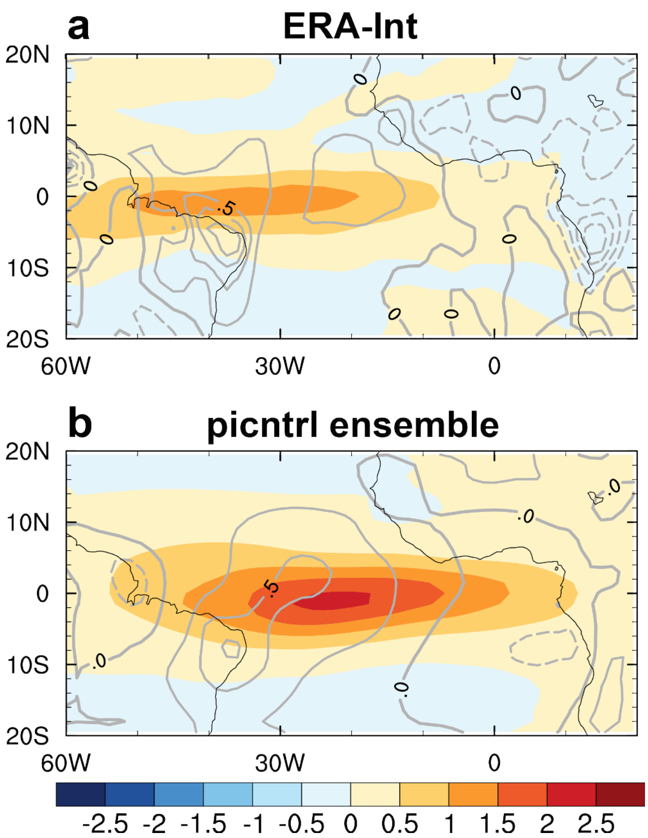

Fig. 6. Anomalous entrainment term (shading; m/s) and pressure gradient term (contours; interval 0.25 m/s) composited on the EAW zonal wind index for **a** ERA-Interim, and **b** the piControl ensemble. The criterion for compositing is +2 standard deviations. Only maxima occurring in MAM are considered.

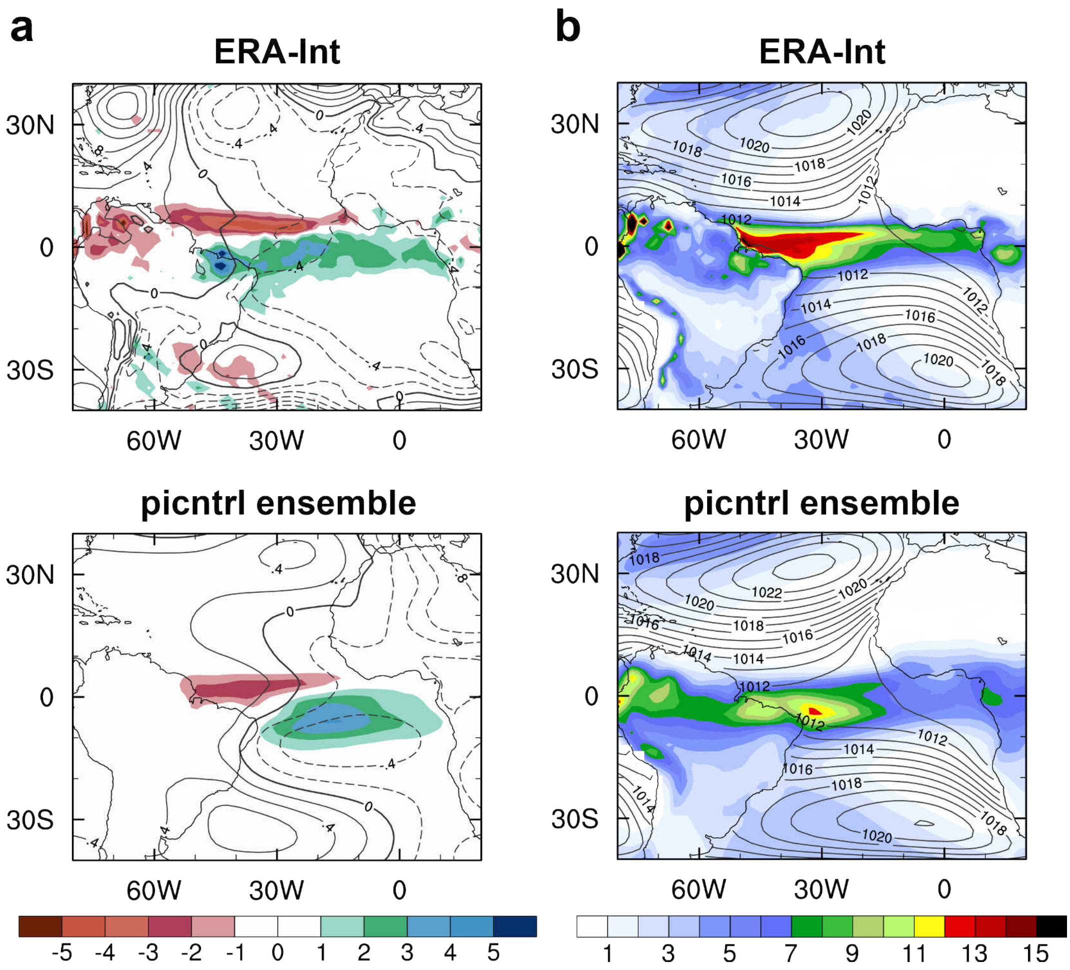

Fig. 7. Precipitation and sea-level pressure fields for the ERA-Interim reanalysis (top row) and the piControl GCM ensemble (bottom row). **a** Precipitation (shading; mm/d) and sea-level pressure (contours; interval 0.1 hPa) anomalies composited on 2 standard deviations of the EAW zonal wind index. **b** Climatological MAM precipitation (shading; mm/d) and sea-level pressure (contours; interval 1 hPa).

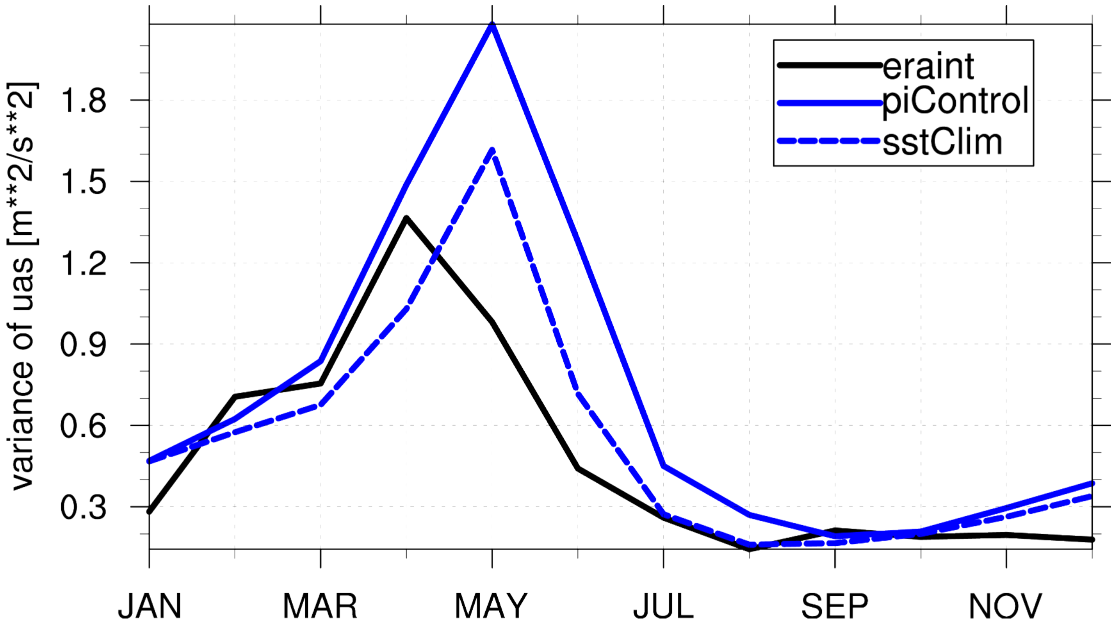

Fig. 8. Variance of zonal winds (m^2/s^2) in the EAW region stratified by month for the ERA-Interim reanalysis (solid black line), the piControl ensemble (solid blue line), and the sstClim ensemble (dashed blue line) in which GCMs are forced with their respective SST climatologies.

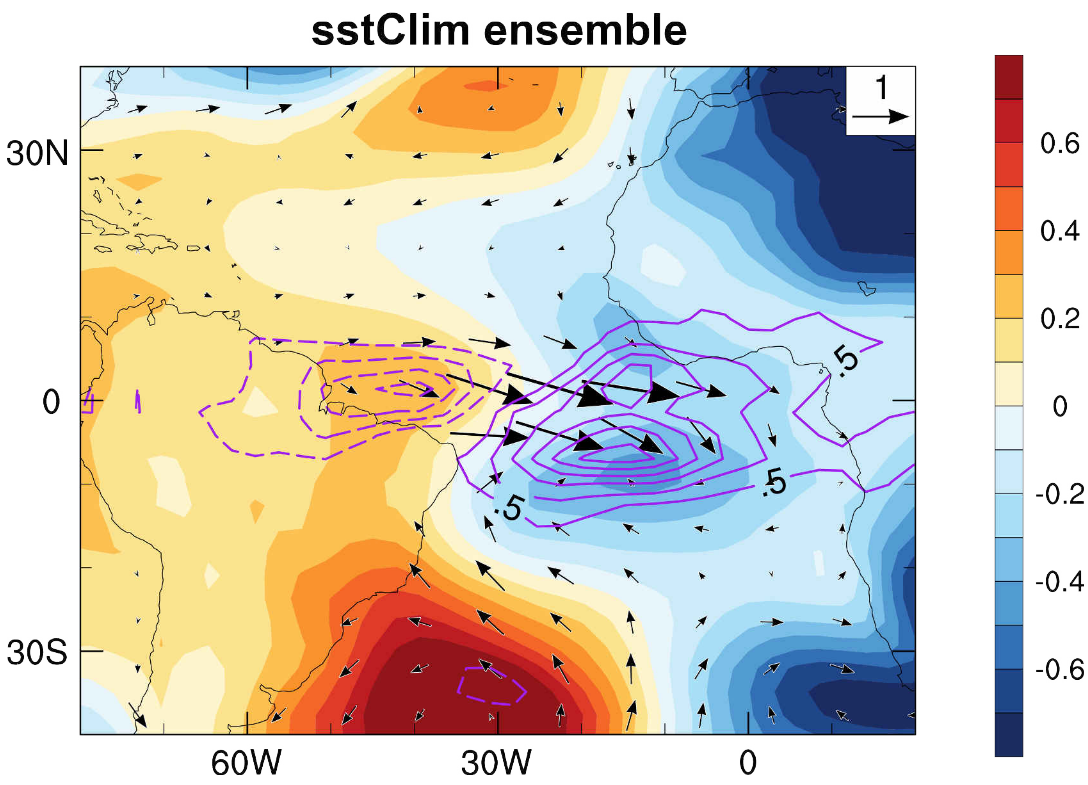

Fig. 9. Anomalous sea-level pressure (shading; hPa), precipitation (contours; interval 0.5 mm/d), and surface winds (vectors; reference 1 m/s) composited on +2 standard deviations the EAW zonal wind index. The figure shows the ensemble average over sstClim GCMs. The analysis is restricted to MAM.

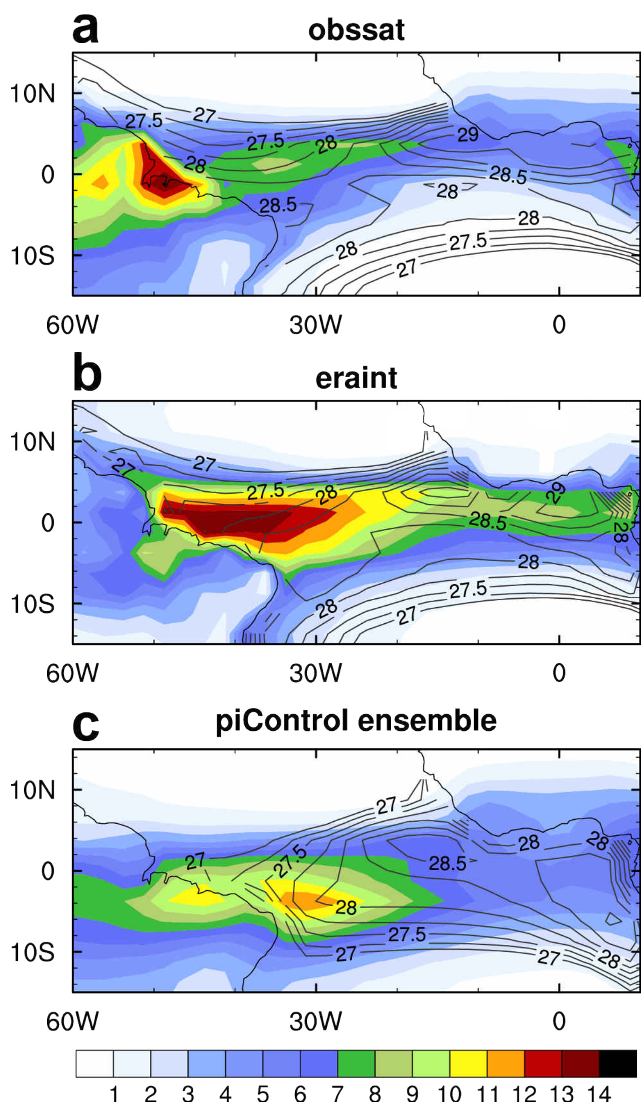

Fig. 10. MAM climatological precipitation (shading; mm/day) and SST (contours; interval 0.5 ºC; contours below 27 ºC are omitted) for **a** AVHRR SST and GPCP precipitation, **b** ERA-Interim reanalysis, and **c** the piControl GCM ensemble.

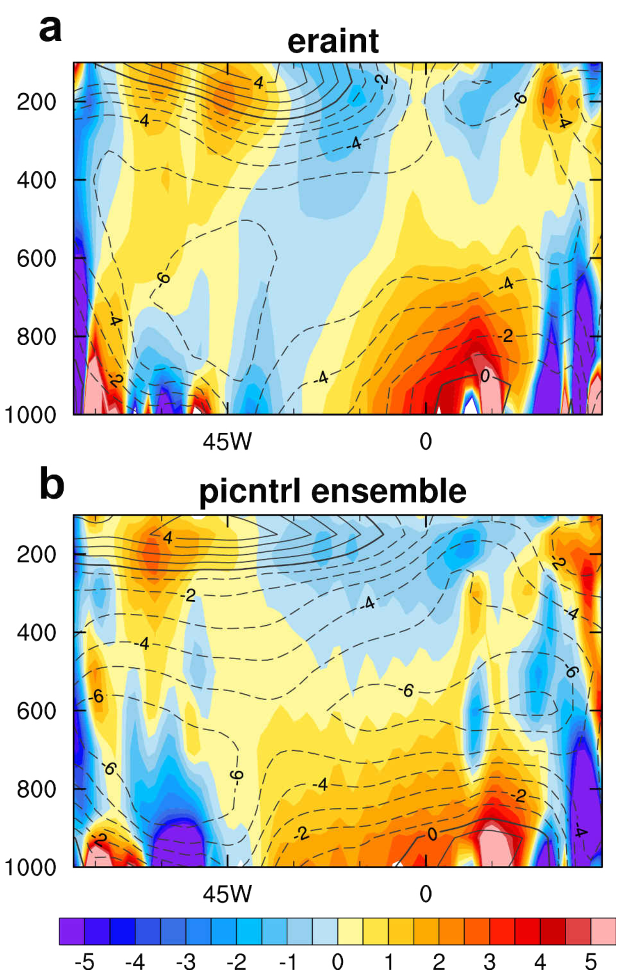

Fig. 11. Longitude-height section of the geopotential height gradient term in the momentum budget (shading; m/s/day), and zonal velocity (contours; intveral 1 m/s) for **a** the ERA-Interim reanalysis, and **b** the piControl ensemble. The fields represent the climatological MAM mean. Negative values of the gradient term correspond to easterly acceleration.